Edinburgh Research Explorer

Formation of supramolecular protein structures on gold surfaces

Link:
[Link to publication record in Edinburgh Research Explorer](#)

Document Version:
Publisher's PDF, also known as Version of record

Published In:
Biointerphases

Formation of supramolecular protein structures on gold surfaces

Laura J. Domigan, Helen Ashmead, Simone Dimartino, Jenny Malmstrom, F. Grant Pearce, Matthew Blunt, David E. Williams, and Juliet A. Gerrard

---

Articles you may be interested in

Adhesion forces of the sea-water bacterium Paracoccus seriniphilus on titanium: Influence of microstructures and environmental conditions
Biointerphases **12**, 05G606 (2017); 10.1116/1.5002676

Quantifying Young's moduli of protein fibrils and particles with bimodal force spectroscopy
Biointerphases **12**, 041001 (2017); 10.1116/1.4996447

Astrocyte spreading and migration on aggrecan–laminin dot gradients
Biointerphases **13**, 01A401 (2018); 10.1116/1.5001675

Silver-, calcium-, and copper molybdate compounds: Preparation, antibacterial activity, and mechanisms
Biointerphases **12**, 05G607 (2017); 10.1116/1.4996434

Enhanced antibacterial activity of silver-ruthenium coated hollow microparticles
Biointerphases **12**, 05G608 (2017); 10.1116/1.5003803

Quartz crystal microbalance with dissipation as a biosensing platform to evaluate cell–surface interactions of osteoblast cells
Biointerphases **13**, 011001 (2018); 10.1116/1.5000752

Formation of supramolecular protein structures on gold surfaces

Laura J. Domigan[a]
School of Biological Sciences, The University of Auckland, Auckland 1010, New Zealand

Helen Ashmead
Callaghan Innovation, Lower Hutt 5010, New Zealand

Simone Dimartino[a]
Institute for Bioengineering, The University of Edinburgh, Edinburgh EH9 3BF, United Kingdom

Jenny Malmstrom[b]
Department of Chemical and Materials Engineering, The University of Auckland, Auckland 1010, New Zealand

F. Grant Pearce[a]
School of Biological Sciences, The University of Canterbury, Christchurch 8041, New Zealand

Matthew Blunt[c]
Department of Chemistry, University College London, London WC1E 6BT, United Kingdom

David E. Williams[b]
The University of Auckland, Department of Chemistry, Auckland 1010, New Zealand

Juliet A. Gerrard[a],[b],[d]
School of Biological Sciences and Department of Chemistry, The University of Auckland, Auckland 1010, New Zealand

Recent research has highlighted the exciting possibilities enabled by the use of protein structures as nanocomponents to form functional nanodevices. To this end, control over protein–protein and protein–surface interactions is essential. In this study, the authors probe the interaction of human peroxiredoxin 3 with gold surfaces, a protein that has been previously identified as having potential use in nanotechnology. Analytical ultracentrifugation and transmission electron microscopy revealed the pH mediated assembly of protein toroids into tubular structures across a small pH range. Quartz crystal microbalance with dissipation measurements showed differences in absorbed protein mass when pH is switched from pH 8.0 to 7.2, in line with the formation of supramolecular structures observed in solution studies. Scanning tunneling microscopy under ambient conditions showed that these protein tubes form on surfaces in a concentration dependent manner, with a tendency for protein adsorption and supramolecular assembly at the edges of Au(111) terraces. Finally, self-assembled monolayer modification of Au surfaces was explored as a means to control the adsorption and orientation of pH triggered protein structures. © *2017 American Vacuum Society.* https://doi.org/10.1116/1.4986053

I. INTRODUCTION

There is a recognized role for biomolecular assemblies in nanotechnology, ranging from DNA origami through to supramolecular protein structures.[1–4] Proteins may be used as building blocks, or tectons, where their natural self-assembly properties are exploited to form valuable architectures. In addition, the diverse chemistry available through the polypeptide chain can be exploited to introduce non-native functionalities in these nanoconstructs.[5–7] The high degree of precision of protein assembly can also be used in a unique way to order other nanocomponents in multiple dimensions,[1,8–10] such as nanoparticle organization for plasmonic devices.[11] In the ordering of nanoscale building blocks for nanodevices such as bioelectronics and biomaterials, protein–surface interactions are an important consideration.[12] Gold surfaces are of particular interest as they can be readily modified via chemisorption of thiol containing compounds under ambient conditions, in order to create protein-reactive surfaces.[13]

A number of challenges are associated with the control of supramolecular protein assemblies, in particular, limitations to their manipulation outside of physiological conditions as well as their structural complexity.[4] Naturally occurring protein assemblies represent an ideal platform to overcome these limitations, enabling the investigation of the formation of these structures via environmental triggers.[14,15] The

---

[a]Present address: Biomolecular Interaction Centre (BIC), Christchurch 8041, New Zealand.
[b]Present address: The MacDiarmid Institute for Advanced Materials and Nanotechnology, Auckland 1010, New Zealand.
[c]Electronic mail: m.blunt@ucl.ac.uk
[d]Electronic mail: j.gerrard@auckland.ac.nz

peroxiredoxin protein family can adopt a wide range of highly ordered quarternary structures, ranging from dimers and toroids,[16,17] to stacks and tubes,[15,18] catenanes,[19] and, under certain conditions, cages.[20] Peroxiredoxins have a number of roles *in vivo*.[21–25] Their ability to function in multiple cellular roles is intrinsically linked to the oligomeric state of the protein.[26] The possibility of predicting conditions that initiate their controlled assembly makes this protein family particularly attractive as a novel protein tecton.[10,15] The peroxiredoxin family has been previously exploited for the formation of composite nanomaterials, such as binding of gold and palladium nanoparticles and to drive the stacking of graphene oxide layers.[8]

In this study, we have used human peroxiredoxin III (*Hs*Prx3), which forms toroidal dodecamers comprising six oblique homodimers.[27] In the native protein, the switch between dimer and dodecamer occurs under nonreducing and reducing conditions, respectively.[15] *p*H changes have an apparent effect on the oligomeric state of peroxiredoxin,[15] with wild type *Hs*Prx3 assembling into 1D tubes at *p*H 4.0.[28] In the current work, we first assessed optimal conditions for the formation of high molecular weight (HMW) species of the tagged human peroxiredoxin III (*Hs*Prx3-6his) using analytical ultracentrifugation (AUC) and transmission electron microscopy (TEM). The inclusion of a tag (which locates to the center of the dodecameric ring) also provides a convenient method for metal binding through chelation to the six histidine residues.[10,29,30]

This study reports the first findings of the surface assembly of *Hs*Prx3-6his. We investigated the interaction of *Hs*Prx3-6his with gold surfaces, with the goal of forming surface tethered supramolecular protein structures that could later be used for the formation of ordered nanoscale assemblies. Scanning tunneling microscopy (STM) under ambient conditions enables the visualization of the morphology of surface immobilized proteins,[31–36] and this, along with quartz crystal microbalance with dissipation (QCM-D), was used to monitor the absorption *Hs*Prx3-6his on gold surfaces. Self-assembled monolayers (SAMs) of functionalized thiols were used as a convenient method to create a protein platform.[13]

II. EXPERIMENT

A. Protein expression and purification

The gene encoding *Hs*Prx3-6his, cloned into pET151-D-TOPO, was synthesized by Epoch Life Science. Chemically competent *Escherichia coli* cells {BL21 (DE3) ROSETTA, Novagen 2013; genotype—F-*ompT hsds*B[B-mB-] *gal dcm* [DE3] pRARE [CamR]} were transformed with the plasmid via heat shock. The protein was successfully expressed in standard lysogeny broth media after shaking (180 rpm) at 37 °C for 4 h, in the presence of ampicillin and chloramphenicol, and then at 26 °C, with the addition of isopropyl *β*-D-1thiogalactopyranoside, for a further 20 h. Cells were lysed via sonication, and the insoluble fraction was removed by centrifugation (18 000*g*, 30 min, 4 °C). *Hs*Prx2-6his was isolated from the soluble crude broth using immobilized metal affinity chromatography (IMAC), and the sample was separated from any remained impurities using size exclusion chromatography (SEC).

B. Analytical ultracentrifugation

Protein solutions were prepared at concentrations ranging from 0.15 to 0.6 mg/ml to a volume of 380 *μ*l. Each sample was analyzed with its own blank (400 *μ*l) containing the corresponding buffer only. Quartz or sapphire cells were used with a path length of 1.2 cm. A wavelength scan was run prior to the experiment to determine the wavelength that provided the optimal optical density ($OD_{270-290}$ between 0.2 and 1.0). The centrifugal velocity was initially set at 38 000 rpm, with samples of a larger molecular weight studied at 20 000 rpm to allow for sedimentation over a greater number of scans. All runs were completed at 20 °C. The Svendberg sedimentation coefficient (*s*) was calculated using the c(s) model in SEDFIT. This software was also used to approximate particle mass using the following equation:[37]

$$M = \frac{s \cdot f \cdot \mathrm{Na}}{1 - \rho \cdot \overline{\upsilon}}, \tag{1}$$

where M = mass, s = sedimentation coefficient; f = frictional coefficient; Na = Avogadro's number; ρ = solvent density; and $\overline{\upsilon}$ = partial specific volume.

C. Transmission electron microscopy

Protein samples were diluted to 50 *μ*g/ml in dH$_2$O immediately prior to grid preparation. Carbon coated formvar 200-mesh copper grids were floated for 1 min on (1) 20 *μ*l protein sample; (2) 20 *μ*l dH$_2$O (×3, 20 s each); and (3) 1% uranyl acetate negative stain. Excess dye was removed using fiberless filter paper. Grids were then air-dried for at least 1 h before TEM analysis. Image collection was carried out on a FEI Morgagni 268D transmission electron microscope operating at 80 kV, with magnifications up to 180 000. Images were captured using a SIS/Olympus Megapixel III digital camera mounted above the phosphor screen.

D. Quartz crystal microbalance with dissipation

1. Preparation of gold surfaces

Gold coated QCM-D crystals (Q-Sense, ATA Scientific, Tarren Point, NSW, Australia) with a fundamental frequency of 4.95 MHz were used. The gold sensors were cleaned with Piranha solution [5:1:1 Milli-Q water, ammonia (25%), hydrogen peroxide (30%)] at 75 °C for 10 min and then rinsed with hot Milli-Q water. The sensors were then dried under nitrogen and placed in an UV/ozone chamber (BioForce Nanosciences) for 10 min.

2. QCM-D experiment

Protein adsorption onto gold surfaces was carried out using a QCM-D system (Q-sense E4 system, Biolin Scientific) equipped with a temperature controlled measuring chamber and a peristaltic pump (ISMATEC® IPC High
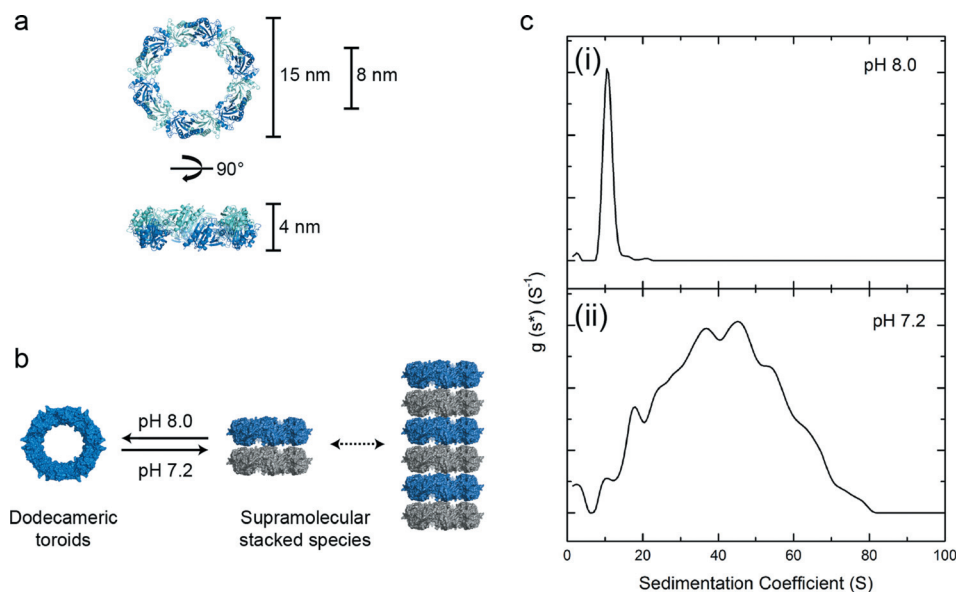
FIG. 1. *p*H triggered assembly in solution. (a) Structure of dodecameric *Hs*Prx3-6his with the monomers highlighted in alternate colors (blue and teal). (b) *Hs*Prx3-6his exists as a dodecameric torroid at *p*H 8.0, which self-associates to form stacked toroids at *p*H 7.2. (c) Analytical ultracentrifugation traces for *Hs*Prx3-6his at (i) *p*H 8.0, and (ii) *p*H 7.2.

Precision Multi channel Dispenser, IDEX Health and Science, Germany). Before each QCM-D experiment, pre-equilibrium with Milli-Q water and then the appropriate buffer was carried out for at least 1 h, in order to reach a stable baseline before the addition of protein solutions. The test solutions were then introduced at a flow rate of 0.1 ml/min. All experiments were carried out at 22 °C.

E. Scanning tunneling microscopy

1. Preparation of gold surfaces

Au(111) substrates consisting of mica slides coated with 300 nm layer of Au metal were purchased from George Albert (BVD-Beschichtungen) and flame-annealed in a butane flame prior to use.

2. 4-MBA SAM formation

Flame-annealed Au(111) substrates were immersed in 100 μM 4-mercaptobenzoic acid (4-MBA) ethanolic solutions overnight. Substrates were then removed from solution, rinsed with solvent, dried under nitrogen. These surfaces were then exposed to protein samples.

3. NTA-thiol functionalization

Flame-annealed Au(111) substrates were floated on a droplet of SH-nitrilotriacetic acid (NTA) (1 mM in 100% ethanol) and incubated in an ethanol vapor chamber for 1.5 h at room temperature. Following this, substrates were washed with 100% ethanol (5–10 min), 70% ethanol, milliQ H_2O (5–10 min), and the appropriate buffer solution (15 min). Surfaces were then incubated in 10 mM $NiCl_2$ (in buffer solution) for 15 min, followed by 2× buffer washes. These surfaces were then exposed to protein samples.

4. STM imaging

Protein samples were deposited onto Au(111) surfaces and allowed to adsorb, followed by rinsing with appropriate buffer solutions and drying under nitrogen. For *in situ* adsorption studies, a polytetrafluoroethylene liquid cell was used and this was filled with the approximately 600 μl protein solution. STM experiments were carried out using a 5500 series SPM system (Keysight Technologies) operating under ambient conditions and at room temperature. STM tips were commercially purchased from Keysight technology and consisted of etched PtIr (80:20) tips coated in apiezon wax with only the tip apex exposed. Each tip was tested prior to use and had a guaranteed <10 pA leakage current. All STM images were subject to a flattening process using the WSXM software package. No additional postprocessing has been applied to the images.

III. RESULTS AND DISCUSSION

A. *Hs*Prx3 forms higher order structures in solution via a *p*H switch

Throughout this study, we have used an N-terminal his-tagged construct of human peroxiredoxin 3 (*Hs*Prx3-6his), with no tag cleavage following purification. Unlike the wild-type protein, the presence of an N-terminal histidine tag on *Hs*Prx3 generates a stable dodecamer in both reducing and nonreducing conditions, providing an ideal tecton from which larger structures can be formed (see supplementary material, Fig. S1).[46] *Hs*Prx3-6his exists as a dodecameric toroid at *p*H 8.0, with an inner and outer diameter of 8 and 15 nm, respectively, with the ring 4 nm in height [Fig. 1(a)]. We have found that in the presence of the N-terminal his-tag, the oligomerization at *p*H 4.0 demonstrated by the wild-type protein is still present (see supplementary material, Fig. S2), but *p*H-triggered assembly and disassembly of stacked

tubes also occurs over a more narrow *p*H range (*p*H 8.0–7.0), offering exciting prospects for the use of the switchable protein tecton over a physiological *p*H range. SEC showed that the switch between single rings and HMW oligomers occurs between *p*H 7.6 and 7.4 (see supplementary material, Fig. S3).

1. Analytical ultracentrifugation

Assembly of *Hs*Prx3 in solution was investigated using AUC across the *p*H range from *p*H 8.0 to 7.2 (see supplementary material, Fig. S4). At *p*H 8.0, there was a predominant species ∼10.5 S [Fig. 1(c), i], close to the expected value for the *Hs*Prx3-6his dodecamer. There was also a small peak at ∼2.5 S which is likely to represent the dimeric species. Decreasing the *p*H to 7.0 triggers the formation of a heterogeneous mixture of large oligomers, which is consistent with the rings stacking to form a tube [Fig. 1(c), ii].

As with the SEC results, the AUC data (Fig. S4) also showed that small changes in *p*H had a large effect on the oligomeric state of *Hs*Prx3-6his, with the shift mainly located between *p*H 7.6 and 7.4. This level of control has not been seen previously for peroxiredoxins.

2. Transmission electron microscopy

Images captured using TEM are in agreement with the solution data. *Hs*Prx3-6his at *p*H 8.0 is present as single rings [Fig. 2(a)], but the degree of oligomerization increases with decreasing *p*H, with the switch from rings to stacks to tubes occurring between *p*H 7.6 and 7.4 (see supplementary material, Fig. S5). At *p*H 7.2, the population is much more heterogeneous, with stacks of two and more present throughout the sample [Fig. 2(b)], and tube size ranging from approximately 10 to 450 nm in length (stacks of 2-112 dodecamers).

B. Assembly of *Hs*Prx3-6his on gold surfaces

The interaction of *Hs*Prx3-6his with surfaces and surface-based formation of supramolecular protein structures was investigated using gold as a model surface. For surface assembly studies, we focused on the *p*H mediated switch between a homogeneous population of single rings (*p*H 8.0), to the assembly of these rings into HMW species including stacked tubes. HMW assembly was monitored at *p*H 7.2 due to the population of single rings being unfavorable at this *p*H [Fig. 1(b)].

1. Quartz-crystal microbalance with dissipation

Real-time monitoring of peroxiredoxin adsorption on gold surfaces was carried out via QCM-D. The time-course of a typical adsorption experiment on gold-coated sensors is shown in Fig. 3. An initial equilibrium step was carried out in the appropriate buffer (*p*H 8.0 or *p*H 7.2) to establish a stable baseline. Solutions containing *Hs*Prx3-6his were then introduced into the system until stable frequency and dissipation signals were obtained. Following this, the sensors
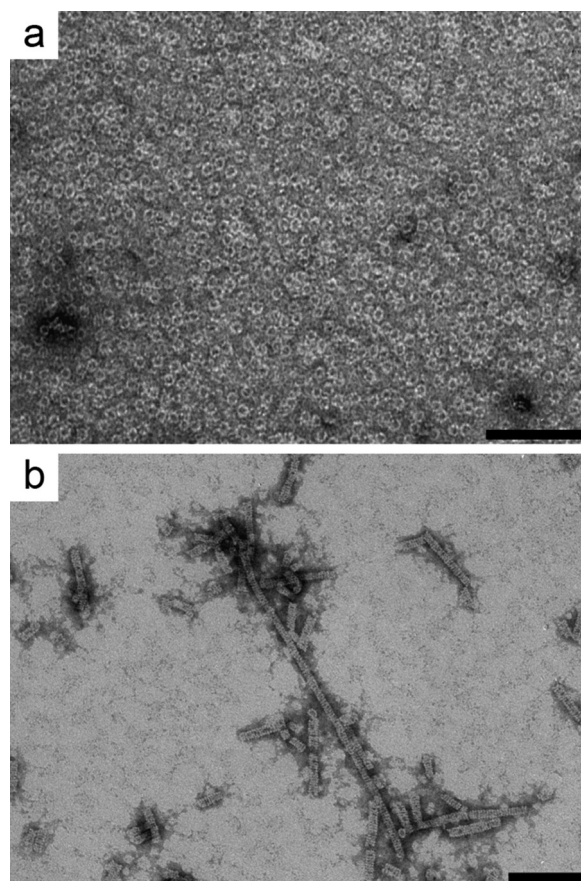

Fig. 2. TEM imaging of *Hs*Prx3-6his. Representative TEM images of *Hs*Prx3-6his at (a) *p*H 8.0 and (b) *p*H 7.2. Scale bars are 100 nm.

were washed with buffer and desorption monitored. The results obtained indicate rapid adsorption of *Hs*Prx3-6his onto gold surfaces. After injection, there was an immediate sharp decrease in the resonance frequency of the QCM sensor, accompanied by a slight increase in dissipation (Fig. 3). Only a small frequency shift is observed following washing of the QCM sensor with buffer. These observations indicate that the protein adsorbs tightly to the underlying gold surface, forming a rigidly bound protein layer.

A greater adsorbed mass (i.e., greater frequency shift) was measured for *p*H 7.2 than *p*H 8.0 at a fixed protein concentration of 10 μg/ml [Fig. 4(a)], as expected due to the presence of HMW species at *p*H 7.2 and the formation of a thicker layer. At *p*H 8.0, where there is a single homogeneous population of toroids, there is no observed concentration dependence of Δ*f* (supplementary material, Fig. S6). This suggests the formation of a protein monolayer, which is independent of the concentration used, indicating the strong adsorption bonds between the gold surface and the protein molecules at *p*H 8.0. At *p*H 7.2, there is an increase in the mass adsorbed when protein concentration is increased to 100 μg/ml (supplementary material, Fig. S6). This is due to the concentration dependence of the equilibrium between heterogeneous species in solution, with increased protein concentration favoring the formation of higher order species, and therefore greater adsorbed mass.
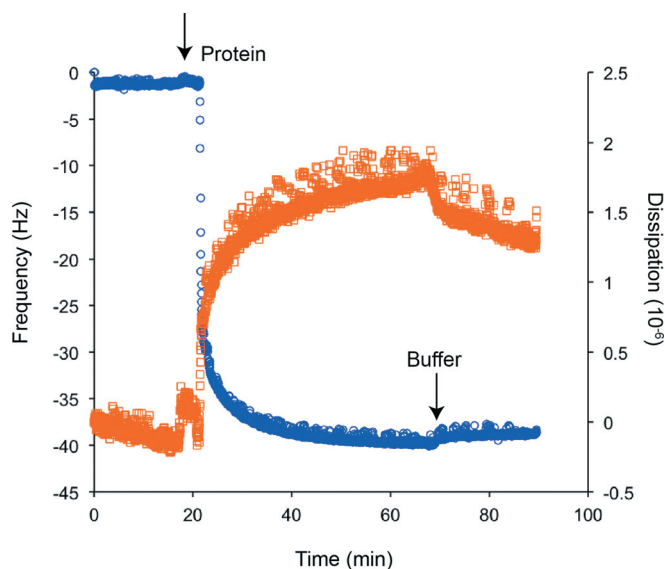
Fig. 3. Representative traces of QCM-D raw data. Frequency (left axis; blue trace) and dissipation (right axis; orange trace) for the ninth overtone of the QCM resonator for *Hs*Prx3-6his adsorption (*p*H 8.0, 0.1 mg/ml) on the Au surface. The first arrow indicates where protein is introduced to the system (following equilibration with buffer) and the second arrow indicates where the buffer wash step commences.

The QCM data are also reported in terms of ΔD vs Δf. Distinctly different curves are apparent at *p*H 8.0 and 7.2 [Figs. 4(b) and 4(c)]. At *p*H 8.0, the slope is relatively constant throughout the experiment, indicating that adsorption of the protein in its dodecameric form follows a similar mechanism, irrespective of the current surface coverage, leading to the formation of a rigid monolayer. At *p*H 7.2, there is an increased slope and two distinct phases, consistent with a rearrangement of the adsorbed stacks and change in their orientation during adsorption, thus facilitating further adsorption of *Hs*Prx3-6his tubes. This supports our hypothesis that the concentration dependent oligomerization seen at this *p*H is also coupled to a rearrangement of protein molecules on the surface.

C. Scanning tunneling microscopy

The formation of high molecular weight species at *p*H 7.2 was further investigated using STM under ambient conditions. *Hs*Prx3-6his was purified at *p*H 8.0 and dialyzed overnight at 4 °C into *p*H 7.2 buffer, as prepared for solution studies. Following this, 10 µl of protein solution was deposited on flame annealed Au(111) on mica substrates and allowed to absorb for 10 min, followed by rinsing with buffer and H$_2$O. STM imaging was carried out under ambient air conditions at the solid–air interface, with images shown in Fig. 5. Representative images obtained at low [5 µg/ml; Fig. 5(A)] and high [50 µg/ml; Fig. 5(B)] protein concentration demonstrate concentration dependent protein oligomerization on surfaces. The images captured show a typical atomically flat area, with the naturally occurring terraces of the Au(111) surface.
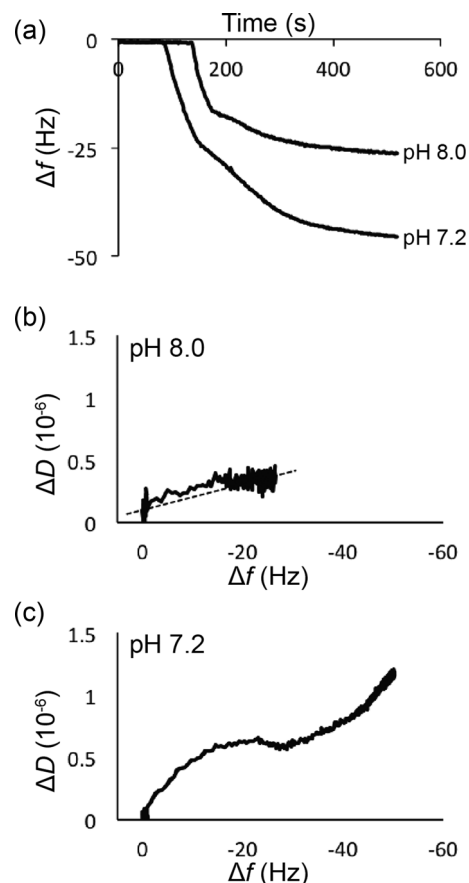

Fig. 4. Plots of QCM-D data for the adsorption of *Hs*Prx3-6his onto unmodified gold surfaces at *p*H 8.0 and *p*H 7.2 (10 µg/ml in appropriate buffer). (a) Representative time-course of Δf for HsPrx3-6his adsorption at *p*H 8.0 and *p*H 7.2. Representative plots of ΔD vs Δf obtained via QCM-D for the adsorption of HsPrx3 onto gold surfaces at (b) *p*H 8.0 (dashed line is linear fit, r^2 = 0.844), and (c) *p*H 7.2.

At low concentration, *Hs*Prx3-6his was visible as discrete "globules" [Fig. 5(A), a and b], with line profiles showing dimensions of approximately 15 nm diameter and 0.5 nm height [Fig. 5(A), a-i, b-i,ii]. This corresponds well to the dimensions of the crystal structure of *Hs*Prx3-6his (PDB 5JCG),[27] when consideration is given for the characteristic decrease in protein heights as measured by STM.[38] This is due to the conductivity of hydrated protein molecules being considerably less than that of the bare gold surface. The theoretical thickness of a dodecamer is 4 nm; STM indicates 0.4 nm so there is an approximate 10× reduction in the size [Fig. 5(A), a-i]. An overlay of line profiles acquired from a number of protein molecules [Fig. 5(A), b-ii] confirms the dimensions to be representative of *Hs*Prx-6his dodecameric rings adsorbed flat on the Au(111) surface [see schematic; Fig. 5(C), a].

At increased protein concentration, association of peroxiredoxin rings into stacks and tubes is observed [Fig. 5(B), a and b]. This is predominantly seen to occur at step edges on the Au(111) surface. Line profiles show increased height (approximately 2 nm). If the approximate 10× reduction in height is accounted for this 20 nm could refer to either

A. pH 7.2, 5 µg/mL

B. pH 7.2, 50 µg/mL

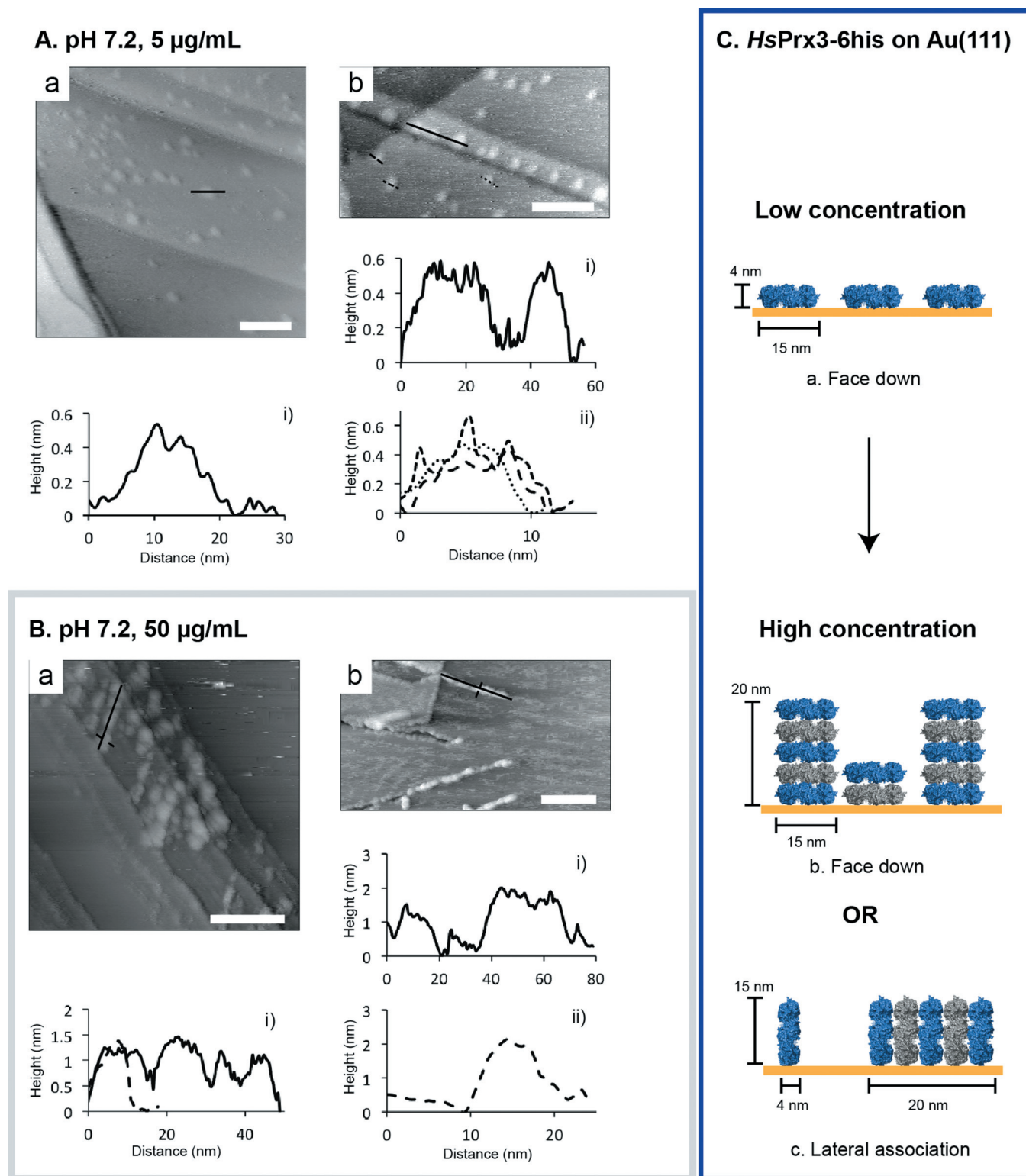## C. *Hs*Prx3-6his on Au(111)

FIG. 5. Assembly of *Hs*Prx3-6his tubes on Au surfaces. STM images obtained of *Hs*Prx3-6his (*p*H 7.2) adsorbed on Au(111) surfaces. Representative STM images obtained at (A) low (5 µg/ml) and (B) high (50 µg/ml) protein concentration. Line profiles correspond to height as a function of distance for the areas indicated in the STM images. Dotted line profiles were taken perpendicular to the solid line profile. (C) Schematic showing the proposed morphology of the adsorbed protein on the gold surface, with concentration dependent protein oligomerization (scale bars 50 nm). Dimensions are taken from the *Hs*Prx3 crystal structure (PDB 5JCG).

stacking of rings on the surface [Fig. 5(C), b], or lateral face-to-face association of *Hs*Prx3-6his rings [Fig. 5(C), c], similar to the structures observed via TEM imaging [Fig. 2(b)]. Line profiles of a tube and its cross-section support this hypothesis [Fig. 5(B), b-i, ii]. Full monolayer coverage was not obtained due to the small volume and time allowed for protein adsorption, necessary to obtain images of individual protein molecules.

D. Controlling the adsorption and orientation of *Hs*Prx3-6his on gold surfaces

The current use of peroxiredoxin as a tecton for the construction of surface nanodevices is limited by a lack of control over its orientation upon adsorption. We seek to form a uniform layer of protein stacks on surfaces, preferably with the central cavity exposed for accessibility to functional cargo into the ring cavity, such as metallic nanoparticles.[10]

Toward this goal, Au surfaces were modified with SAMs to investigate methods to control the adsorption and orientation of *Hs*Prx3-6his on Au surfaces.

1. SAM formation on gold surfaces

Au was modified with (1) 4-MBA and (2) NTA-thiol conjugated to Ni^{2+} ions [see supplementary material (Fig. S7)]. 4-MBA forms well characterized SAMs on gold surfaces.[39] Formation upon Au surfaces results in a protein reactive surface due to the presence of free carboxy groups that interact with available amines on the protein surface (Fig. S7), with amide bond formation in the presence of 1-ethyl-3-(3-dimethylaminopropyl) carbodiimide N-hydroxysuccinimide (EDC-NHS).

NTA-thiol SAM formation results in the surface availability of a NTA group, which forms a tetravalent chelate with Ni^{2+}. His-tagged proteins, such as the *Hs*Prx3-6his construct used in this study, bind via the interaction of histidine with surface immobilized Ni^{2+} ions, similar to the interactions used in IMAC. This method results in the formation of a semipermanent protein layer, which can be removed via displacement with metal ions or imidazole. The above SAMs were successfully formed on Au(111) surfaces and imaged using STM (Fig. S8).

2. Assembly of HsPrx3-6his on SAM modified surfaces

STM imaging of *Hs*Prx3-6his adsorbed on Au(111) surfaces modified with MBA SAMs showed a number of globules, representative of protein immobilized on the Au surface [Fig. 6(A), a]. The lack of movement of the globules with repeated scanning indicated that they were covalently bound (via EDC-NHS) to the surface, and the presence of the cross-linker appears to give better dispersion of the protein on the surface.[40] Line profiles show discrete globules to have dimensions of approximately 15 nm diameter and heights ranging from 0.5 to 2.4 nm, indicative of peroxiredoxin rings bound face down on the surface [Fig. 6(A), a-ii]. In some images it was possible to visualize the central hole, supporting the above hypothesis [Fig. 6(A), a-ii]. *Hs*Prx3-6his will covalently bind to the MBA surface via EDC-NHS mediated amide bond formation predominantly utilizing surface accessible lysine residues, of which there are a number on the ring top and base [Fig. S7]. Based on dimensions measured for single rings (0.4 nm height; Fig. 5), it appears that *Hs*Prx3-6his is predominantly bound face down on the surface with vertical stacking occurring, consisting of approximately one to six laterally associating protein rings.

To promote further stacking of peroxiredoxin rings, Au substrates "preseeded" with *p*H 7.2 *Hs*Prx3-6his, as described above, were then exposed to *p*H 4.0 HsPrx3-6his [Fig. 6(A), b]. At *p*H 4.0 amide bond formation is less favorable and the formation of *Hs*Prx3-6his stacks is promoted (Fig. S2). Histograms of height constructed from particle analysis carried out on STM images show that this strategy resulted in the increased growth of protein columns on the surface (up to 4 nm in height) [Fig. 6(A), b-iii], compared to 2 nm stacks for those surfaces only exposed to the *p*H 7.2 protein [Fig. 6(A), a-iii].

Another strategy employed to immobilize peroxiredoxin stacks was via nickel complexed NTA-thiol SAMs. This also resulted in *Hs*Prx3-6his immobilization, via interaction with the his-tag in the central ring cavity. In this case, discrete protein globules were also visualized [Fig. 6(B), i]. Under these conditions, there appeared to be less bound protein and for it to predominantly exist as single rings [Fig. 6(B), ii], with histograms showing limited stack formation [Fig. 6(B), iii]. Based on our hypothesis that the his-tag mediates stacking at *p*H 7.2, we think this is due to competing interactions between his-tags on adjacent dodecamers, and the his-tag with the surface immobilized nickel. However, as mentioned previously, this immobilization strategy results in a semipermanent protein layer, with bound peroxiredoxin rings able to be displaced by high imidazole concentrations. This property could be exploited in later studies, or binding efficiency improved through chelation of cobalt in place of nickel.[41]

IV. SUMMARY AND CONCLUSIONS

*Hs*Prx3 with a his-tag (*Hs*Prx3-6his) was shown via AUC and TEM to assemble into stacked toroids over a narrow physiological *p*H range (*p*H 7.2–8.0), in contrast to the untagged protein that forms tubes at *p*H 4.0. While the exact mode of oligomerization is at this stage unclear, control over high molecular weight assembly of *Hs*Prx3-6his through small changes in *p*H places this protein as an ideal tecton for the formation of biological nanomaterials.

Having gained control of assembly in solution we are beginning to develop strategies to create organized 2D structures on surfaces. Nonspecific protein adsorption on surfaces can lead to protein unfolding and desorption over time. Coupling via functional groups (such as amines and thiols), present at exposed surface amino acid residues, provides an easy method of surface immobilization. However, even such coupling usually results in unspecific binding and random protein orientation at the interface. Specific binding interactions, such as biotin–strepavidin, or through incorporation of un-natural amino acids and purification tags, provide a means by which protein–surface interactions can be predicted and to some extent controlled, and generally lead to minimal protein denaturation upon adsorption.[41–45]

Investigation into the assembly of *Hs*Prx3-6his on Au surfaces showed *p*H triggered supramolecular structures also formed on surfaces, as monitored by ambient STM and QCM-D. SAM modification (4-MBA and NTA-thiol
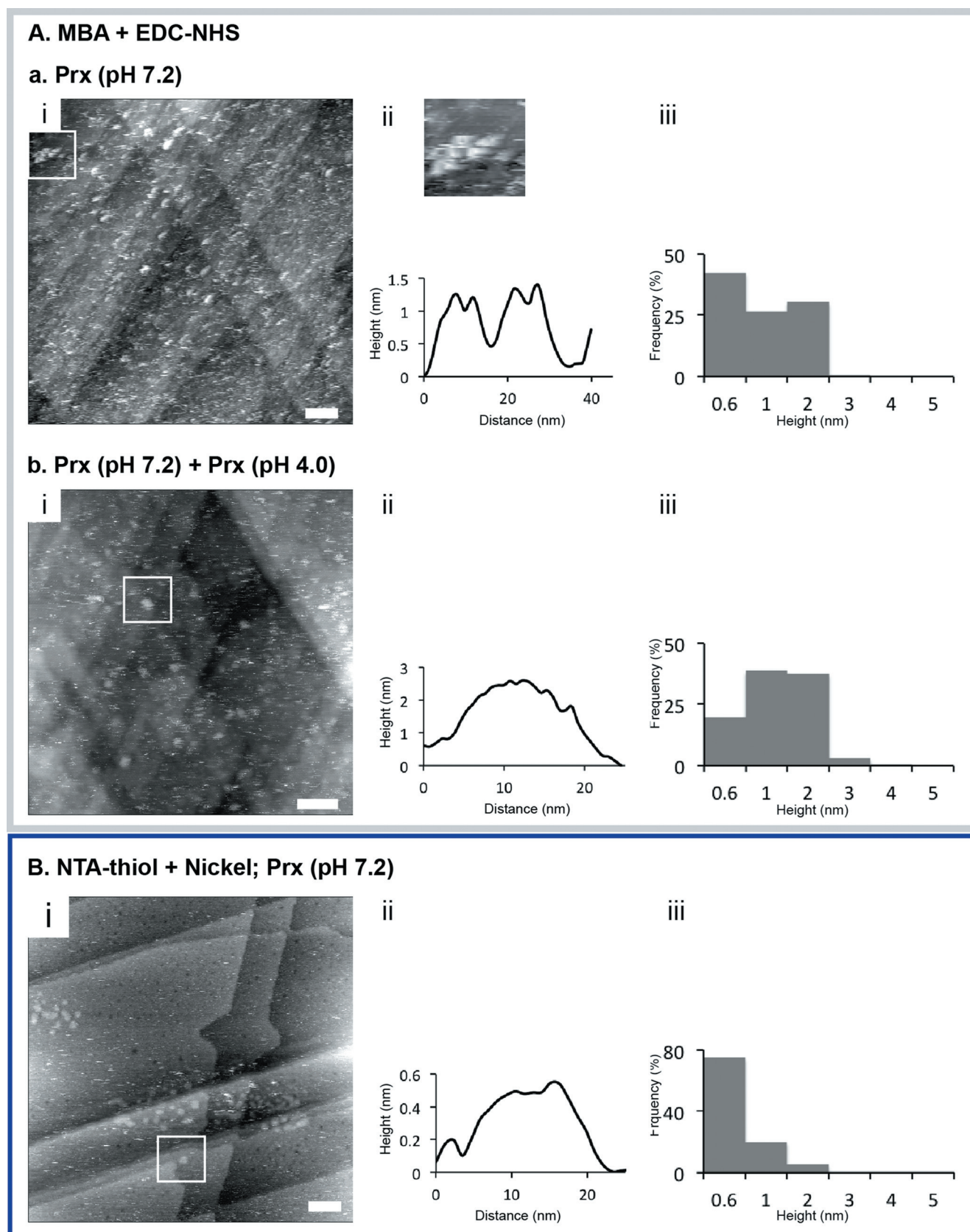
A. MBA + EDC-NHS

a. Prx (pH 7.2)

b. Prx (pH 7.2) + Prx (pH 4.0)

B. NTA-thiol + Nickel; Prx (pH 7.2)

FIG. 6. SAM mediated assembly of *Hs*Prx3-6his stacks. Peroxiredoxin stacks were formed on Au(111) surfaces via immobilization of *Hs*Prx3-6his (*p*H 7.2) to SAMs formed from (A) MBA (in the presence of EDC-NHS), and (B) NTA-thiol (complexed to nickel). (i) Representative STM images of surface immobilized *Hs*Prx3-6his (scale bars 50 nm). (ii) Line profiles corresponding to height as a function of distance for the areas indicated in the STM images. (iii) Histograms of HsPrx3-6his stack height from particle analysis of STM images.

chelated Ni^{2+}) of Au surfaces was used as a means to control the adsorption and orientation of protein tubes on surfaces. This presents the first critical step in surface assembly of this protein tecton, toward its use for the ordering of nanocomponents.

ACKNOWLEDGMENTS

[1] I. Medalsy, O. Dgany, M. Sowwan, H. Cohen, A. Yukashevska, S. G. Wolf, A. Wolf, A. Koster, and O. Almog, Nano Lett. **8**, 473 (2008).

[2] S. M. Douglas, H. Dietz, T. Liedl, B. Hogberg, F. Graf, and W. M. Shih, Nature **459**, 414 (2009).

[3] P. W. K. Rothemund, Nature **440**, 297 (2006).

[4] Y. Kim and Y. Jung, Org. Biomol. Chem. **14**, 5352 (2016).

[5] H. Inaba, N. J. M. Sanghamitra, K. Fujita, T. Sho, T. Kuchimaru, S. Kitagawa, S. Kizaka-Kondoh, and T. Ueno, Mol. Biosyst. **11**, 3111 (2015).

[6] Y. E. Kim, Y. Kim, J. A. Kim, H. M. Kim, and Y. Jung, Nat. Commun. **6**, 7134 (2015).

[7] H. Sun, X. Zhang, L. Miao, L. Zhao, Q. Luo, J. Xu, and J. Liu, ACS Nano **10**, 421 (2016).

[8] M. Ardini *et al.*, Nanoscale **8**, 6739 (2016).

[9] J. Malmstroem, A. Wason, F. Roache, N. A. Yewdall, M. Radjainia, S. Wei, M. J. Higgins, D. E. Williams, and J. A. Gerrard, Nanoscale **7**, 19940 (2015).

[10] M. Ardini, F. Giansanti, L. Di Leandro, G. Pitari, A. Cimini, L. Ottaviano, M. Donarelli, S. Santucci, and F. Angelucci, Nanoscale **6**, 8052 (2014).

[11] R. P. M. Hoeller, M. Dulle, S. Thoma, M. Mayer, A. M. Steiner, S. Forster, A. Fery, C. Kuttner, and M. Chanana, ACS Nano **10**, 5740 (2016).

[12] A. J. Zaitouna and R. Y. Lai, Anal. Chim. Acta **828**, 85 (2014).

[13] G. M. Whitesides, J. P. Mathias, and C. T. Seto, Science **254**, 1312 (1991).

[14] H. M. Ashmead, L. Negron, K. Webster, V. Arcus, and J. A. Gerrard, Biopolymers **103**, 260 (2015).

[15] A. J. Phillips, J. Littlejohn, N. A. Yewdall, T. Zhu, C. Valery, F. G. Pearce, A. Mitra, M. Radjainia, and J. A. Gerrard, Biomacromolecules **15**, 1871 (2014).

[16] A. Hall, P. A. Karplus, and L. B. Poole, FEBS J. **276**, 2469 (2009).

[17] Z. A. Wood, L. B. Poole, R. R. Hantgan, and P. A. Karplus, Biochemistry **41**, 5493 (2002).

[18] F. Saccoccia, P. Di Micco, G. Boumis, M. Brunori, I. Koutris, A. E. Miele, V. Morea, P. Sriratana, and D. L. Williams, Structure **20**, 429 (2012).

[19] Z. Cao, D. P. McGow, C. Shepherd, and J. G. Lindsay, PLoS One **10**, e0123303 (2015).

[20] U. Meissner, E. Schroder, D. Scheffler, A. G. Martin, and J. R. Harris, Micron **38**, 29 (2007).

[21] P. A. Karplus, Free Radic. Biol. Med. **80**, 183 (2015).

[22] A. Perkins, K. J. Nelson, D. Parsonage, L. B. Poole, and P. A. Karplus, Trends Biochem. Sci. **40**, 435 (2015).

[23] M. Banerjee, D. Chakravarty, and A. Ballal, BMC Plant Biol. **15**, 444 (2015).

[24] A. G. Cox, C. C. Winterbourn, and M. B. Hampton, Biochem. J. **425**, 313 (2010).

[25] A. Perkins, L. B. Poole, and P. A. Karplus, Biochemistry **53**, 7693 (2014).

[26] A. Hall, K. Nelson, L. B. Poole, and P. A. Karplus, Antioxid. Redox Signaling **15**, 795 (2011).

[27] N. A. Yewdall, H. Venugopal, A. Desfosses, V. Abrishami, Y. Yosaatmadja, M. B. Hampton, J. A. Gerrard, D. C. Goldstone, and A. K. Mita, Structure **24**, 1120 (2016).

[28] M. Radjainia, H. Venugopal, A. Desfosses, A. J. Phillips, N. A. Yewdall, M. B. Hampton, J. A. Gerrard, and A. K. Mitra, Structure **23**, 912 (2015).

[29] N. Ferrer-Miralles, J. L. Corchero, P. Kumar, J. A. Cedano, K. C. Gupta, A. Villaverde, and E. Vazquez, Microb. Cell. Fact. **10**, 101 (2011).

[30] S. V. Wegner, F. C. Schenk, and J. P. Spatz, Chem. Eur. J. **22**, 3156 (2016).

[31] S. A. Contera, H. Iwasaki, and S. Suzuki, Ultramicroscopy **97**, 65 (2003).

[32] L. Haggerty and A. Lenhoff, Biophys. J. **64**, 886 (1993).

[33] S.-U. Kim, Y. J. Kim, S.-G. Choi, C.-H. Yea, R. P. Singh, J. Min, B.-K. Oh, and J.-W. Choi, Ultramicroscopy **108**, 1390 (2008).

[34] S. A. Contera and H. Iwasaki, Ultramicroscopy **91**, 231 (2002).

[35] I. I. Rzeznicka, G. W. H. Wurpel, M. Bonn, M. A. van der Horst, K. J. Hellingwerf, S. Matsunaga, T. Yamada, and M. Kawai, Chem. Phys. Lett. **472**, 113 (2009).

[36] A. F. Raigoza, J. W. Dugger, and L. J. Webb, ACS Appl. Mater. Interfaces **5**, 9249 (2013).

[37] P. Schuck, Biophys. J. **78**, 1606 (2000).

[38] H. M. Yusoff, I. I. Rzeznicka, H. Hoshi, S. Kajimoto, N. N. Horimoto, K. Sogawa, and H. Fukumura, Appl. Surf. Sci. **280**, 776 (2013).

[39] S. Creager and C. Steiger, Langmuir **11**, 1852 (1995).

[40] E. E. Bedford, S. Boujday, V. Humblot, F. X. Gu, and C.-M. Pradier, Colloid Surf. B **116**, 489 (2014).

[41] J. F. Young, H. D. Nguyen, L. Yang, J. Huskens, P. Jonkheijm, and L. Brunsveld, ChemBioChem **11**, 180 (2010).

[42] P. Jonkheijm, D. Weinrich, H. Schroeder, C. M. Niemeyer, and H. Waldmann, Angew. Chem. Int. Ed. **47**, 9618 (2008).

[43] A. Gonzalez-Campo, M. Brasch, D. A. Uhlenheuer, A. Gomez-Casado, L. Yang, L. Brunsveld, J. Huskens, and P. Jonkheijm, Langmuir **28**, 16364 (2012).

[44] A. Syguda, A. Kerstan, T. Ladnorg, F. Stuben, C. Woll, and C. Herrmann, Langmuir **28**, 6411 (2012).

[45] A. Turchanin, A. Tinazli, M. El-Desawy, H. Grobmann, M. Schnietz, H. H. Solak, R. Tampe, and A. Golzhauser, Adv. Mater. **20**, 471 (2008).

[46] See supplementary material at http://dx.doi.org/10.1116/1.4986053 for further details of HsPrx3-6his oligomerisation (SEC, AUC, TEM, QCM-D) and SAM formation.